Molecular Dynamics Investigation of Halide-Containing Phospho-Silicate Bioactive Glasses

Alfonso Pedone,[a,*] Xiaojing Chen[b,c], Robert G. Hill[c], Natalia Karpukhina[c]

[a]Dipartimento di Scienze Chimiche e Geologiche, Università di Modena e Reggio Emilia, Via G. Campi 103, 41125 Modena, Italy

[b] Xiangya Stomatological Hospital & School of Stomatology, Central South University, Changsha, Hunan 410078, P.R. China

[c]Dental Physical Sciences, Institute of Dentistry, Queen Mary University of London, Mile End Road, London E1 4NS, United Kingdom

AUTHOR INFORMATION:

Corresponding Author

*E-mail: alfonso.pedone@unimore.it

Abstract.

Oxyhalide-containing silicate glasses receive an increasing attention in recent years due to their extensive medical and dental applications.

This manuscript reports the first detailed structural investigation using MD simulations in the context of chloride and mixed fluoride/chloride containing phosphosilicate bioactive glasses. It is shown that adding fluoride, chloride and mixed fluoride and chloride have not altered the Q^n silicate distribution and phosphorus speciation significantly in all the glasses investigated. The Q^2 silicon species is the predominant species with smaller and nearly equal proportions of Q^1 and Q^3 species whereas phosphorous is largely present as orthophosphate Q^0 units. No Si-F/Cl and P-F/Cl bonds have been observed at room temperature. Both F and Cl anions are present as F-Ca(n) and Cl-Ca(n). MD simulations also indicate the opposite effects of fluoride and chloride on crystallisation ability of the glasses. The environment of Cl in chloride containing glass series is quite different from the chlorapatite and $CaCl_2$ crystals and a significant structural re-organisation is required to observe the appearance of the crystals nuclei. Instead, the environment of fluoride ions in the glasses is quite similar to that present in the FAP and CaF_2 crystals and thus F-containing glasses manifest a high crystallisation tendency. Moreover, in the mixed fluoride/chloride-containing glasses, fluorine tends to surround phosphate whereas chloride moves towards the silicate network. Finally, it was observed that a good correlation exists between the glass transition temperature and the overall strength of the glass network quantified by the F_{net} factor.

Introduction

Bioactive glasses (BGs) were the first synthetic materials possessing the bioactivity, which means they degrade in physiological media and form an apatite-like phase bonding to bone and thus promoting new bone formation[1]. The first bioactive glass (Bioglass 45S5) with the composition of 46.1SiO_2 - 2.6P_2O_5 - 24.4Na_2O - 26.9CaO (in mol%) was designed in late 70s and it has been clinically used since 1985.

In the recent years, halide-containing BGs have attracted a great attention for their potential applications in medicine and dentistry, for instance, using as the main therapeutic agents in re-mineralizing toothpastes[2,3] and resorbable bone grafting materials.[4]

The most investigated halogen in silicate glass is fluoride. It has been introduced into BGs for instance by Brauer *et al.*[5] and Chen *et al.*[6] to reduce glass firing temperature (T_{firing}) and glass transition temperature (T_g). As a results of its incorporation into bioactive glass fluoride led to increase glass bioactivity by promoting the formation of acid-durable fluoroapatite (FAP), which is particularly attractive for dental applications. However, the concept of 'the more the better' is not suitable for the optimisation of glass properties by introducing fluoride. It was found that the uncontrolled crystallisation of the fluoride-containing crystalline phases including FAP, cuspidine, fluorite occurred at the fluoride content equal or higher than 9.3 mol%. Consequently, the release of fluoride ions from glasses, which is required for FAP formation, was suppressed, resulting in a reduction in glass bioactivity.[6]

Chloride, which belongs to the same halogen group as fluoride, has been introduced alternatively into the glass with composition of 38.1SiO_2 – 55.5CaO – 6.3P_2O_5 (in mol%).[4,7] Interestingly, it was shown that all the equivalent chloride-containing glasses were largely amorphous. Similar to fluoride, the incorporation of chloride made no significant change in the glass Q^n silicate network structure but led to a remarkable decrease in T_{firing} and T_g.

Moreover, Chen *et al.*[3] found that the glass degradation rate increased with an increase in chloride content. A rapid hydroxyapatite-like phase formation was found within 3 hours immersion in Tris buffer for all the chloride-containing glasses in contrast to fluoride-containing glasses where FAP formed upon immersion.[8]

To exploit the potential of combining the benefits of both halogens into one composition, we have synthesised a series of mixed fluoride/chloride-containing BGs.[9] We observed that the properties of mixed bioactive glasses are influenced from the presence of both CaF_2 and $CaCl_2$, which showed some similarities to those of the singly doped glasses. For instance, the glass transition temperature decreases with the CaX_2 content whereas the molar volume increases with the CaX_2 content leading to glasses more easily degradable.

Regarding the crystallisation tendency, it was observed that the mixed glasses were partially and spontaneously crystallised to FAP during quenching at the lowest halide content compared to the singly fluoride or chloride doped glasses, meantime CaF_2 was detected in glasses with high CaF_2 content (> 9.2%). This is contradictive to the expectation that the mixed glasses were crystallised less readily compare to the fluoride containing glasses, since chloride showed the ability to inhibit glass crystallisation. The relationship between the glass atomic structure and their tendency of crystallisation is particularly interesting, yet it remains poorly understood.

It is believed that glass properties are largely determined by the glass structure. For the mixed fluoride/chloride-containing BGs, the Q^n silicate distribution and the structural role of fluoride and phosphate have been investigated by ^{29}Si, ^{19}F and ^{31}P MAS-NMR.[9] Unlike the ^{19}F nuclide, which has a nuclear spin number of 1/2, a high gyromagnetic ratio and a 100% natural isotopic abundance, the low gyromagnetic ratio, the large quadrupole moment and the relatively low resonance frequency of ^{35}Cl nuclide lead to broad and indiscernible signals.

Therefore, using ^{35}Cl MAS-NMR to evaluate the atomic environment of chloride in BGs is very challenging.

Classical molecular dynamics (MD) simulations have been successfully used in the last decades to gain insights into the short and medium range structure of multicomponent glasses[10–21]. Furthermore, the MD simulations could provide an indirect interpretation and corroborate the NMR results when it is difficult to acquire high resolution NMR spectra of glasses. Pedone *et al.*[22–24] used MD simulation and Density Functional Theory (DFT) calculations to elucidate the structural role of fluorine in a 45S5 based bioactive glass, which has 10 mol% CaO been substituted with CaF_2. Fluorine was found almost entirely coordinated to network modifier cations Na^+ and Ca^{2+} and no appreciable amount of Si-F bonds were present in the glass structure. Moreover, our simulations revealed that upon CaF_2 addition a phase separation between a silica rich region and micro segregation zones rich in metals (Ca and F) and fluorine ions occurred.

Instead, core-shell MD simulations were performed very recently by Swansbury *et al.*[25] to investigate the structural role of chlorine and the onset of phase separation in chloride-containing calcium metasilicate glasses developed by Chen *et al.*[26]. Additionally, Chungong *et al.*[27] used neutron diffraction to evaluate the structural role of chlorine in the same compositions. Both MD simulations and neutron diffraction found that chlorine was predominantly coordinated with calcium and there was an absence of Si-Cl bonding, which showed a good agreement with the ^{29}Si MAS-NMR carried out previously.[3]

However, the aforementioned chloride-containing glasses are phosphate free. To the best of our knowledge, there is no structural investigation of chloride or mixed fluoride/chloride-containing BGs with the presence of phosphate by using MD simulations.

Therefore, in this manuscript, we developed new self-consistent core-shell force-fields parameters for F- and Cl- anions in silicate based BGs and reported the first detailed structural investigation of chloride- and mixed fluoride/chloride-containing BGs using MD simulations.

Computational details.

The new self-consistent core-shell force fields parameters were used to investigate the atomic scale structure of the mixed halide CaO-SiO_2-P_2O_5 bioactive glasses (GPFCl2.6, GPFCl5.3, GPFCl12.2 and GPFCl23.6) as well as the structure of only fluoride-containing BGs (GPF3.0, GPF6.0, GPF13.6, GPF25.5) and only chloride-containing BGs (GPCl2.3, GPCl4.6, GPCl10.6, GPCl20.6) synthesized and experimentally characterised in the previous works by Chen *et al.*[9] whose compositions are reported in Table 1. Molecular dynamics simulations were carried out by using the DL_POLY® package[28] employing a well-established melt-quench computational protocol.[13]

Initial random configurations containing about 10,000 atoms enclosed in a periodic cubic box with the experimental density were melted at 3200 K and then cooled down to 300 K at a nominal cooling rate of 5 K/ps. The resulting glass structures have been subjected to a final NVT trajectory of 0.3 ns; and the structural analysis was performed on 501 configurations sampled at regular intervals during the last 0.2 ns of MD trajectory.

The force field used is based on the adiabatic core-shell model in which the most polarizable ions, O^{2-}, F^- and Cl^-, are split between a core bearing almost all the mass and a positive charge, X, and a shell bearing a negative charge, Y (X + Y = Q, the formal charge).

The core and shell are coupled by a harmonic spring potential of the form:

$$U_{c-s}(r) = \frac{k_{c-s}}{2}(r_{c-s})^2 \quad (1)$$

Short range interactions between shells were modelled with a Buckingham potential, while long range core-core, core-shell and shell-shell electrostatic interactions were modelled with a Coulomb potential:

$$U(r_{ij}) = k\frac{q_i q_j}{r_{ij}} + A_{ij} \cdot \exp(-r_{ij}/\rho) - \frac{C_{ij}}{r_{ij}^6} \quad (2)$$

A three-body screened harmonic potential was used to guide O-Si-O and O-P-O, Cl-Si-Cl and F-Si-F intra-tetrahedral angles to the value typical of a tetrahedral coordination (θ_{ijk}^0 = 109.7°)

$$U(\theta_{ijk}) = \frac{k_b}{2}(\theta_{ijk} - \theta_{ijk}^0)^2 \cdot \exp\left(-\frac{r_{ij}}{\rho_b} - \frac{r_{ik}}{\rho_b}\right) \quad (3)$$

The parameters for O^{2-}, Si^{4+}, P^{5+} and Ca^{2+} were taken from the literature whereas those for F and Cl- were parametrized in this work since none of F^- parameters found in the literature[29,30] was totally consistent with Si/P-O potential parameters. Regarding the chlorine parameters, at the time we started our investigation there were no parameters and thus we developed our own set.

As for fluoride parameters, we adopted the F_c-F_s charge split presented by Catlow et al.[29], which was recently employed to successfully simulate alkali-free Sr ,Zn co-doped bioactive glasses.[31]

The harmonic constant k_{c-s}^F was then calculated according to the relationship between polarizability (α) and k_{c-s} ($\alpha = (Y)^2/k_{c-s}$) by using a value for a^{F-} proportional to that of a^{O2-} in the force-field, according to the ratio a^{O2-}/a^{F-} calculated at the DFT level of theory with the Gaussian code[32]. Subsequently, GULP code[33] allowed us to perform a relaxed fitting[34] of A, ρ and C Buckingham potentials for P-F_s, Si-F_s, Ca-F_s, F_s-F_s and F_s-O_s atom pairs. The fitting was carried on PF_5 and SiF_4 (optimized at the DFT-B3LYP/6311+G(d,p) level with the Gaussian code), on CaF_2 and $Ca_4Si_2O_7F_2$ experimental structures taken from the MINCRYST database.[35]

Concerning Chloride parameters, the Cl_c-Cl_s charge split was taken from ref.[36] whereas the harmonic constant k_{c-s}^{Cl} was computed analogously to that of fluoride ions.

As before, the values of A, ρ and C parameters of the Buckingham potentials for P-Cl_s, Si-Cl_s, Ca-Cl_s, Cl_s-Cl_s and Cl_s-O_s atom pairs were fitted on PCl_5 and $SiCl_4$ molecules (optimized at the DFT-B3LYP/6311+G(d,p) level with the Gaussian code), on $CaCl_2$, Ca_2SiO_4 $CaCl_2$ and $Ca_{12}Si_4O_{16}Cl_8$ structures taken from the MYNCRYST database. All the force field potential forms and parameters are reported in **table 2**.

Before using these parameters to investigate the structure of fluoride and chloride glasses we have tested their reliability by carrying out a relaxed geometry optimization of several reference crystalline phases.

Table S1 and **S2** of the ESI report cell parameter, average bond length (<X-Y>, X=Na/Ca/Si/P and Y=F/Cl/O) and bond length (X-Y) variations after the optimization of CaF_2, SiF_4, PF_5, $Ca_4Si_2O_7F_2$, $CaCl_2$, $SiCl_4$, PCl_5, $Ca_2SiO_4{\cdot}CaCl_2$ and $Ca_{12}Si_4O_{16}Cl_8$ crystal phases. Volume variations never exceed +1.8%, and average bond lengths are reproduced within 0.05 Å in all cases. Coordination geometry is always correctly reproduced, and particular bond distance varies within 0.06 Å. The relative percentage variation on average bond lengths is ≤ 3 % in most cases. Exceptions are *i)* two P-Cl bonds in PCl_5 molecule (+0.09 Å, +4%) and *ii)* one Ca-O bond in Ca(2) site (+0.11 Å, +4%) of $Ca_{12}Si_4O_{16}Cl_8$. The relative percentage variation on bond length is acceptable to guarantee the simulation of sound structural models of glasses.

Results and Discussion.

Short-range Order. The short-range order of the investigated glasses have been studied by analysing the M-O and M-X (M=Si, P and Ca, X= F, Cl) pair distribution functions (PDFs) that provide bond distances and if properly integrated the coordination number (CN) of each cation with all the anions.

The average bond distances and coordination numbers of Si, P, Ca, Cl and F species in the investigated glass series are reported in **Table 3**. In all models, all P atoms and Si atoms show a tetrahedral coordination. Average Si-O and P-O bonds lengths were measured 1.61-1.62 Å and 1.55 Å, respectively, in perfect agreement with experimental data[37] and the previous computational works[38–41] on bioactive glasses. In agreement with other classical and Car-Parrinello MD simulations on fluoride-containing glasses[22,24] no Si-F/Cl and P-F/Cl bonds have been found within the models at room temperature denoting that both halogens prefer to interact with calcium than network former cations.

Figure 1 reports the Ca-O, Ca-F and Ca-Cl PDFs for the GPFCl23.6 glass since the features of PDFs are similar for all three glass series simulated. The figure reveals that Ca-F bonds are shorter than Ca-O, which in turn are shorter than the Ca-Cl ones. The Ca-F PDFs are also narrower than the others denoting a better-defined environment when Ca ions are coordinated by fluoride ions.

In all glasses, the Ca-O bond distance range between 2.32 and 2.34 Å and Ca-F bond distances range between 2.20 and 2.23 Å. Regarding the Ca-Cl bond distances we have observed a bond shortening from 2.77 to 2.74 Å with the $CaCl_2$ content in the GPCl series and a lengthening from 2.74 to 2.77 Å in the GPFCl series. In both cases, the values of the Ca-Cl distances are aligned with experimental values in $CaCl_2$ crystals (Table S3 of ESI) and with the MD results by Swansbury *et al.*[25]

In the GPCl series both Cl and O coordinate calcium to a varying degree depending on the glass composition. By increasing $CaCl_2$ content, Ca coordination by O decreases from 6.1 for GPCl2.3 to 4.4 for GPCl20.6, whereas the number of Cl^- ions surrounding Ca^{2+} increases from 0.3 to 2.4. On average Cl^- ions are coordinated by 4.4 Ca^{2+} ions in GPCl2.6 and the coordination decreases slightly with the $CaCl_2$ content reaching the value of 4.3 for GPCl20.6. Instead, the coordination number remains between 4.5 and 4.6 in the mixed

GPFCl series. In both $CaCl_2$ and ClAP crystals, Cl^- is coordinated by 3 Ca^{2+}.[42] It is clear that the environment of Cl in the glasses and the relevant crystals is quite different. This characteristic could explain the absence of crystallisation nuclei in the bulk of chloride-containing alkali-free BGs under study observed experimentally.[3]

Regarding the GPF series, our simulations reveal that by increasing CaF_2 content, Ca coordination by O decreases from 6.0 to 4.0 for GPF3.0 and GPF25.5 glasses, whereas the number of F^- ions coordinating Ca^{2+} increases from 0.4 to 2.7 respectively. The total coordination number of Ca^{2+} ions (computed by using a cutoff of 3.0 Å) increases from 6.4 to 6.7. The average coordination number of F^- ions in terms of Ca^{2+} ions slightly increases with the addition of CaF_2 from 3.4 for GPF3.0 to 3.6 for GPF25.5. Similar coordination number and bond distances are observed for the GPFCl glass series. In CaF_2, F^- is coordinated by 4 Ca^{2+} ions, while F^- is coordinated by 3 Ca^{2+} cations in FAP. Therefore, unlike the Cl case, there is more similarity for the F environment in GPF and GPFCl glasses and the relevant crystals. In fact, at low CaF_2 contents the F environment is more similar to the one in FAP whereas at high CaF_2 contents the F environment is more similar to that of fluorite. These observations are in agreement with the high crystallisation tendency observed for the glasses containing fluoride reported in the previous experimental works.[8,9]

The short-range order has been also investigated by analysing the bond angle distributions (BADs) of particular triplets of atoms. The O-Si-O and O-P-O BADs are very similar to those reported for other phospho-silicate BGs in the past and thus they have not been reported and discussed here. Figure 2 reports the Si-O-Si, P-O-Si and O/F/Cl-Ca-O/F/Cl BADs of the GPF25.5, GPCl20.6 and GPFCl23.6 glasses. The fluoride-containing glasses presents a smaller Si-O-Si angle (129°) and a narrower distribution with respect to the chloride-containing glasses for which the Si-O-Si BAD is centered at about 132°.

The P-O-Si angles are centered at about 132° for all glasses, although the GPF25.5 glass shows a narrower distribution. It seems that the fluoride-containing glasses are more 'ordered' and better 'packed' than the chloride-containing glasses. These features are in agreement with the experimental observations shown that the chloride-containing glasses are largely amorphous and the molar volumes of chloride-containing glasses are larger than that of fluoride-containing glasses.

The three series of glasses have very similar O-Ca-O BADs, which exhibit a peak close to 80°, resulting from Ca atoms connecting with two NBOs belonging to different tetrahedral and a second peak at 60° resulting from modifiers coordinated to two NBOs belonging to the same tetrahedron. This distribution is in line with those findings for other bioactive glass compositions.[10,38] Interestingly, the O-Ca-Cl and O-Ca-F BADs are very similar with a major peak centered at 74-75°, whereas some differences are encountered for the Cl-Ca-Cl and F-Ca-F BADs though it must be noted that the statistic is a bit poorer for such triplets. The curves have similar shapes but the F-Ca-F angles are smaller (73°) than the Cl-Ca-Cl ones (82°) in accordance with the radius of the two anions and the number of halogens coordinated to Ca ions. The Cl-Ca-Cl BAD of the GPFCl23.6 glass presents an additional peak centered at 134° better defined than that of the GPCl20.6 glass suggesting that the addition of fluorine ions in chloride-containing glasses can lead to more ordered Cl sites than that observed in chloride-containing glasses without the presence of fluoride. Once again, this is in agreement with the increased crystallisation tendency of mixed halide-containing BGs observed experimentally.[9]

Medium-range order. The analysis of the medium-range order has revealed that as expected the Q^2 silicon species is the predominant species (50-52%) in all the investigated glasses with nearly equal proportion 21-25% of Q^1 and Q^3 species. The NC is constant at around 2.00 as expected for these compositions and their values together with the Q^n distributions are

reported in **Table 4**. The Q^0 orthophosphate units represents the vast majority of P arrangement, their percentage in the chloride-containing glasses decreases with the addition of $CaCl_2$ from 80.5% in GPCl2.3 to 72.5% in GPCl20.6. In addition, there is around 20% Q^1 phosphate speciation assigned to Si-O-P linkages. A small fraction of Q^1 phosphorus species was also obtained from the computations for other two series of glasses. To some extent, this is in accordance with the ^{31}P MAS-NMR spectra for the three series of glasses reported previously,[7,9] which exhibited some asymmetry in the chemical shift range of Q^1 pyrophosphate, though its estimated fraction is much lower than the Q^1 computed in this work. However, it is worth remembering that MD-derived structural models have a high effective fictive temperature, which results in a more disordered structure than that found experimentally. Therefore, the amount of Q^1 species is possibly overestimated in our MD simulations.

The arrangement of cations around themselves has been investigated by computing the cation-cation CNs within a cutoff of 5.0 Å. The results for the three series of glasses are reported in Table 5. By adding CaF_2 in the GPF series the Si-Ca CN slightly increases from 7.9 (GPF3.0) to 8.2 (GPF25.5); the P-Ca CN increases from 8.9 to 9.8, the Si-F CN increases from 0.9 to 6.5 whereas the P-F CN increases from 1.0 to 8.5. The prominent increment in the number of Ca^{2+} and F^- ions around P seems to indicate the formation of CaF_2-orthophosphate rich domains. In the GPFCl glass series we found that the CN of Si-F is smaller than that of Si-Cl through the whole series, while the CN of P-F is larger than that of P-Cl. Moreover, similar to the GPF glass series, a more pronounced increase in the CN of P-Ca and P-F were found compared with the CN of Si-Ca and Si-F. Thus, a conclusion can be made that in the GPFCl glass series, the CaF_2-orthophosphate rich domains form preferentially against $CaCl_2$-orthophosphate rich domains.

Focusing on Ca second coordination sphere in GPF series it is possible to observe a more pronounced depletion of Si (Ca-Si CN decreases from 5.1 to 3.6) than P atoms (Ca-P CN decreases from 1.9 to 1.4) and a concurrent large clustering of Ca^{2+} ions (Ca-Ca CN increases from 7.5 to 9.1, data reported in Table S3 of ESI). Similar trends are seen in the GPFCl series. In addition, the increase in the P-F CN is more pronounced compared with the equivalent in P-Cl CN, indicating that the orthophosphate is more likely surrounded by a larger amount of CaF^{+} species. Different trends are found in the GPCl series for which both the number of Ca surrounding SiO_4 and PO_4 units slightly decreases with the addition of $CaCl_2$ while Ca-Ca CN slightly varies from 7.4 (GPCl2.3) to 7.6 (GPCl20.6).

All these observations and the graphical representation of the GPF25.5 and GPCl20.6 glasses in Figure 3 reveal that heterogeneities are observed in these glasses. In both cases, calcium halide type domains (rich in F^- and /or Cl^- ions) hosting some PO_4 tetrahedral, calcium phosphate rich zones and calcium silicate domains are present. Ca^{2+} seems to act as buffer between silicate network and CaF_2 and $CaCl_2$ phosphate depolymerized region. The intermixing between F^- and Cl^- ions around SiO_4 and PO_4 units in the GPFCl series has been also investigated by computing the ratio:

$$R_T^{F/Cl} = \frac{CN_T^F}{CN_T^{Cl}} \times \frac{N_{Cl}}{N_F}$$

where T=Si or P; CN_T^X is the number of X^- ions around the T atom. If $R_T^{F/Cl}$ is greater than 1, this indicates that F is preferably located around T with respect to Cl; if it is smaller than 1, the opposite is true. The obtained value of 0.8 and 1.2-1.3 for $R_{Si}^{F/Cl}$ and $R_P^{F/Cl}$ respectively in all GPFCl glasses demonstrates that when both halogens are present in the glass F tends to surround P whereas Cl moves towards the silicate network as shown in **Figure 4**. This also shows an agreement with the observation of FAP in the mixed fluoride/chloride-containing BGs.

QSPR model for the glass transition temperature. A great advantage of molecular dynamics simulations is that it can provide a plethora of structural descriptors that can be correlated to macroscopic properties of interest such as glass transition temperature and durability. The simplest structural descriptors are bond, angles, coordination numbers, percentage of bridging oxygens, network connectivity etc.. Other more complex descriptor can be defined as the combination of the aforementioned structural descriptors with other physicochemical data.

A few years ago, one of us shown that a descriptor that estimates the overall strength of the glass network indicated as F_{net} is able to explain the trends of the glass transition temperature and chemical durability of different glass compositions.[43] F_{net} is defined by the following equation:

$$\boldsymbol{F_{net} = \frac{1}{N}\left[\sum_{i}^{cations}\sum_{j}^{anions} n_i \cdot CN_{ij} \cdot BE_{ij} \cdot m_{ij}\right]} \quad (4)$$

where N is the number of atoms in the simulation box, $\boldsymbol{n_i}$ is the number of cations of the i-th species, $\boldsymbol{CN_{ij}}$ is then mean coordination number of the i-j pairs of atoms (i =Si, P, Ca; j = O,F,Cl). $\boldsymbol{BE_{ij}}$ are the gas phase bond enthalpies for each type of bond in the corresponding molecules reported in ref.[44] and $\boldsymbol{m_{ij}}$ are multiplicative factors that take into account the maximum number of SiO_4 and PO_4 units linked to i-j bonds ($\boldsymbol{m_{SiO} = 4}$; $\boldsymbol{m_{SiX} = 3}$; $\boldsymbol{m_{PO} = 3}$; $\boldsymbol{m_{PX} = 2}$; $\boldsymbol{m_{CaO} = 2}$; $\boldsymbol{m_{CaX} = 1}$, $\mathbf{X = F\ or\ Cl}$).[45]

Figure 5 shows that a good linear correlation (R^2=0.95) is observed between the experimental T_g taken from ref.[9] and the computed F_{net} factor of the glasses investigated. In general, the addition of halogen ions leads to a reduction of the overall network strength and thus to a reduction of the glass transition temperature. As shown previously, the attempt to correlate the T_g values to the F_{net} computed by considering only the Si-O and P-O bonds

provides much worst correlations. This was expected since the network connectivity of silicon is very similar for all the glasses as well as the Q^n speciation of phosphorous, which is present dominantly as Q^0 species. Therefore, the contribution of cations-halogens bonds in the F_{net} is fundamental for the prediction of the experimental behaviour of halide-containing glasses.

Conclusions.

This is the first time that classical MD simulations were employed to understand the glass structure and properties in the context of chloride and mixed fluoride/chloride-containing phospho-silicate bioactive glasses. The studied glasses present a heterogeneous structure at the atomic level. It has been revealed that all the studied glasses present a glass structure dominated by Q^2 silicon species with small and nearly equal proportions of Q^1 and Q^3 silicon species. Phosphorous is largely present as orthophosphate. There is an absence of Si-F/Cl and P-F/Cl bonds in all three series of glasses. Both fluorine and chlorine tend to coordinate calcium cations forming F-Ca(n) and Cl-Ca(n) species that strongly affect the medium-range order and the properties, such as the glass transition temperature. It was also observed that fluorine tends to surround phosphate whereas chloride moves towards the silicate network in the mixed fluoride/ chloride-containing glasses. Due to the fact that the environment of chloride in the glasses differs from those in ClAP and $CaCl_2$ crystals and a significant structural re-organisation is required to observe the appearance of crystalline phase, while the environment of fluoride in the glasses is quite similar to those present in FAP and CaF_2 crystals, the chloride-containing BGs manifest a low tendency of crystallisation, while a different case is found in the fluoride-containing BGs.

Interestingly, we have also observed that the QSPR approach, introduced in a previous work,[43] was tested on halogen containing glass series investigated. We found that the overall

network strength quantified by the F_{net} factor that take into accounts the contribution of all glass components linearly correlates with important technological properties such as the glass transition temperature.

Supporting Information

The supporting information is available free of charge on the ACS Publication website. The comparison between the experimental and computed unit cell parameters and bond lengths of F- and Cl-containing crystalline phases are reported in Tables S1 and S2, respectively. The Ca-Ca, P-Si, Si-P, P-P and Si-Si coordination numbers of the investigated glasses are reported in Table S3.

Acknowledgments

AP thanks Elisa Gambuzzi for her contribution in the development of some FF parameters. Dr. Xiaojing Chen's PhD was sponsored by China Scholarship Council (CSC)/Queen Mary University of London Joint PhD scholarships.

References.

(1) Brauer, D. S. Bioactive Glasses—Structure and Properties. *Angew. Chem. Int. Ed.* **2015**, *54* (14), 4160–4181.

(2) Shah, F. A. Fluoride-Containing Bioactive Glasses: Glass Design, Structure, Bioactivity, Cellular Interactions, and Recent Developments. *Mater. Sci. Eng. C Mater. Biol. Appl.* **2016**, *58*, 1279–1289.

(3) Chen, X.; Karpukhina, N.; Brauer, D. S.; Hill, R. G. High Chloride Content Calcium Silicate Glasses. *Phys. Chem. Chem. Phys.* **2017**, *19* (10), 7078–7085.

(4) Chen, X.; Karpukhina, N.; Brauer, D. S.; Hill, R. G. Novel Highly Degradable Chloride Containing Bioactive Glasses. *Biomed. Glas.* **2015**, *1* (1).

(5) Brauer, D. S.; Karpukhina, N.; O'Donnell, M. D.; Law, R. V.; Hill, R. G. Fluoride-Containing Bioactive Glasses: Effect of Glass Design and Structure on Degradation,

pH and Apatite Formation in Simulated Body Fluid. *Acta Biomater.* **2010**, *6* (8), 3275–3282.

(6) Chen, X.; Chen, X.; Brauer, D. S.; Wilson, R. M.; Hill, R. G.; Karpukhina, N. Novel Alkali Free Bioactive Fluorapatite Glass Ceramics. *J. Non-Cryst. Solids* **2014**, *402* (Supplement C), 172–177.

(7) Chen, X.; Hill, R.; Karpukhina, N. Chlorapatite Glass-Ceramics. *Int. J. Appl. Glass Sci.* **2014**, *5* (3), 207–216.

(8) Chen, X.; Chen, X.; Brauer, D. S.; Wilson, R. M.; Hill, R. G.; Karpukhina, N. Bioactivity of Sodium Free Fluoride Containing Glasses and Glass-Ceramics. *Materials* **2014**, *7* (8), 5470–5487.

(9) Chen, X.; Chen, X.; Pedone, A.; Apperley, D.; Hill, R. G.; Karpukhina, N. New Insight into Mixing Fluoride and Chloride in Bioactive Silicate Glasses. *Sci. Rep.* **2018**, *8* (1), 1316.

(10) Tilocca, A. Structural Models of Bioactive Glasses from Molecular Dynamics Simulations. *Proc. R. Soc. Lond. Math. Phys. Eng. Sci.* **2009**, *465* (2104), 1003–1027.

(11) Tilocca, A. Models of Structure, Dynamics and Reactivity of Bioglasses: A Review. *J. Mater. Chem.* **2010**, *20* (33), 6848–6858.

(12) Ori, G.; Montorsi, M.; Pedone, A.; Siligardi, C. Insight into the Structure of Vanadium Containing Glasses: A Molecular Dynamics Study. *J. Non-Cryst. Solids* **2011**, *357* (14), 2571–2579.

(13) Pedone, A. Properties Calculations of Silica-Based Glasses by Atomistic Simulations Techniques: A Review. *J. Phys. Chem. C* **2009**, *113* (49), 20773–20784.

(14) Pedone, A.; Menziani, M. C.; Cormack, A. N. Dynamics of Fracture in Silica and Soda-Silicate Glasses: From Bulk Materials to Nanowires. *J. Phys. Chem. C* **2015**, *119* (45), 25499–25507.

(15) Du, J.; Corrales, L. R. Structure, Dynamics, and Electronic Properties of Lithium Disilicate Melt and Glass. *J. Chem. Phys.* **2006**, *125* (11), 114702.

(16) Du, J.; Xiang, Y. Effect of Strontium Substitution on the Structure, Ionic Diffusion and Dynamic Properties of 45S5 Bioactive Glasses. *J. Non-Cryst. Solids* **2012**, *358* (8), 1059–1071.

(17) Gambuzzi, E.; Pedone, A. On the Structure of Ce-Containing Silicophosphate Glasses: A Core–shell Molecular Dynamics Investigation. *Phys. Chem. Chem. Phys.* **2014**, *16* (39), 21645–21656.

(18) Kokou, L.; Du, J. Rare Earth Ion Clustering Behavior in Europium Doped Silicate Glasses: Simulation Size and Glass Structure Effect. *J. Non-Cryst. Solids* **2012**, *358* (24), 3408–3417.

(19) Christie, J. K.; Ainsworth, R. I.; de Leeuw, N. H. Investigating Structural Features Which Control the Dissolution of Bioactive Phosphate Glasses: Beyond the Network Connectivity. *J. Non-Cryst. Solids* **2016**, *432* (Part A), 31–34.

(20) Christie, J. K.; Ainsworth, R. I.; Di Tommaso, D.; de Leeuw, N. H. Nanoscale Chains Control the Solubility of Phosphate Glasses for Biomedical Applications. *J. Phys. Chem. B* **2013**, *117* (36), 10652–10657.

(21) I. Ainsworth, R.; K. Christie, J.; Leeuw, N. H. de. On the Structure of Biomedical Silver-Doped Phosphate-Based Glasses from Molecular Dynamics Simulations. *Phys. Chem. Chem. Phys.* **2014**, *16* (39), 21135–21143.

(22) Lusvardi, G.; Malavasi, G.; Cortada, M.; Menabue, L.; Menziani, M. C.; Pedone, A.; Segre, U. Elucidation of the Structural Role of Fluorine in Potentially Bioactive Glasses by Experimental and Computational Investigation. *J. Phys. Chem. B* **2008**, *112* (40), 12730–12739.

(23) Pedone, A.; Charpentier, T.; Menziani, M. C. The Structure of Fluoride-Containing Bioactive Glasses: New Insights from First-Principles Calculations and Solid State NMR Spectroscopy. *J. Mater. Chem.* **2012**, *22* (25), 12599–12608.

(24) Christie, J. K.; Pedone, A.; Menziani, M. C.; Tilocca, A. Fluorine Environment in Bioactive Glasses: Ab Initio Molecular Dynamics Simulations. *J. Phys. Chem. B* **2011**, *115* (9), 2038–2045.

(25) Swansbury, L. A.; Mountjoy, G.; Chen, X.; Karpukhina, N.; Hill, R. Modeling the Onset of Phase Separation in $CaO–SiO_2–CaCl_2$ Chlorine-Containing Silicate Glasses. *J. Phys. Chem. B* **2017**, *121* (22), 5647–5653.

(26) Chen, X. Novel Halide Containing Bioactive Glasses. Thesis, Queen Mary University of London, 2015.

(27) Forto Chungong, L.; Swansbury, L. A.; Mountjoy, G.; Hannon, A. C.; Lee, A. F.; Martin, R. A. Atomic Structure of Chlorine Containing Calcium Silicate Glasses by Neutron Diffraction and 29Si Solid-State NMR. *Int. J. Appl. Glass Sci.* **2017**, *8* (4), 383–390.

(28) Smith, W.; Forester, T. R. DL_POLY_2.0: A General-Purpose Parallel Molecular Dynamics Simulation Package. *J. Mol. Graph.* **1996**, *14* (3), 136–141.

(29) Catlow, C. R. A.; Diller, K. M.; Norgett, M. J. Interionic Potentials for Alkali Halides. *J. Phys. C Solid State Phys.* **1977**, *10* (9), 1395.

(30) Sangster, M. J. L.; Atwood, R. M. Interionic Potentials for Alkali Halides. II. Completely Crystal Independent Specification of Born-Mayer Potentials. *J. Phys. C Solid State Phys.* **1978**, *11* (8), 1541.

(31) Goel, A.; Kapoor, S.; Tilocca, A.; Rajagopal, R. R.; Ferreira, J. M. F. Structural Role of Zinc in Biodegradation of Alkali-Free Bioactive Glasses. *J. Mater. Chem. B* **2013**, *1* (24), 3073–3082.

(32) *M. J. Frisch, G. W. Trucks, H. B. Schlegel, G. E. Scuseria, M. A. Robb, J. R. Cheeseman, G. Scalmani, V. Barone, B. Mennucci, G. A. Petersson, et al. , Gaussian 09 (Gaussian, Inc., Wallingford CT, 2009).*

(33) Gale, J. D. GULP: Capabilities and Prospects. *Z. Für Krist. - Cryst. Mater.* **2009**, *220* (5/6), 552–554.

(34) Gale, J. D. Empirical Potential Derivation for Ionic Materials. *Philos. Mag. Part B* **1996**, *73* (1), 3–19.

(35) WWW-MINCRYST - CRYSTALLOGRAPHIC DATABASE FOR MINERALS http://database.iem.ac.ru/mincryst/ (accessed Sep 18, 2017).

(36) Binks, D. J. Computational Modelling of Zinc Oxide and Related Oxide Ceramics. doctoral, University of Surrey, 1994.

(37) FitzGerald, V.; Pickup, D. M.; Greenspan, D.; Sarkar, G.; Fitzgerald, J. J.; Wetherall, K. M.; Moss, R. M.; Jones, J. R.; Newport, R. J. A Neutron and X-Ray Diffraction Study of Bioglass® with Reverse Monte Carlo Modelling. *Adv. Funct. Mater.* **2007**, *17* (18), 3746–3753.

(38) Pedone, A.; Malavasi, G.; Menziani, M. C. Computational Insight into the Effect of CaO/MgO Substitution on the Structural Properties of Phospho-Silicate Bioactive Glasses. *J. Phys. Chem. C* **2009**, *113* (35), 15723–15730.

(39) Malavasi, G.; Pedone, A.; Menziani, M. C. Study of the Structural Role of Gallium and Aluminum in 45S5 Bioactive Glasses by Molecular Dynamics Simulations. *J. Phys. Chem. B* **2013**, *117* (15), 4142–4150.

(40) Tilocca, A.; Cormack, A. N.; de Leeuw, N. H. The Structure of Bioactive Silicate Glasses: New Insight from Molecular Dynamics Simulations. *Chem. Mater.* **2007**, *19* (1), 95–103.

(41) Xiang, Y.; Du, J. Effect of Strontium Substitution on the Structure of 45S5 Bioglasses. *Chem. Mater.* **2011**, *23* (11), 2703–2717.

(42) Hughes, J.; Cameron, M.; Crowley, K. Structural Variations in Natural F, Oh, and Cl Apatites. *Am. Mineral.* **1989**, *74* (7–8), 870–876.

(43) Lusvardi, G.; Malavasi, G.; Tarsitano, F.; Menabue, L.; Menziani, M. C.; Pedone, A. Quantitative Structure−Property Relationships of Potentially Bioactive Fluoro Phospho-Silicate Glasses. *J. Phys. Chem. B* **2009**, *113* (30), 10331–10338.

(44) Haynes, W. M. *CRC Handbook of Chemistry and Physics, 95th Edition*; CRC Press, 2014.

(45) Hill, R. G.; Costa, N. D.; Law, R. V. Characterization of a Mould Flux Glass. *J. Non-Cryst. Solids* **2005**, *351* (1), 69–74.

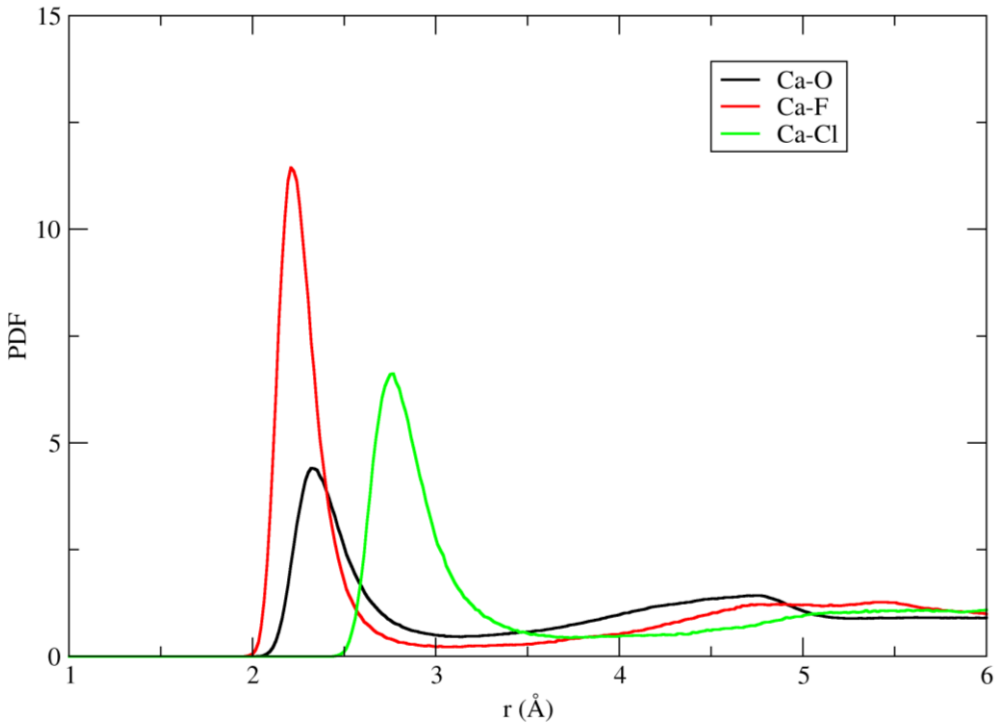

Figure 1. Pair distribution functions for the Ca-O, Ca-F and Ca-Cl atom pairs in the GPFCl23.6 glass.

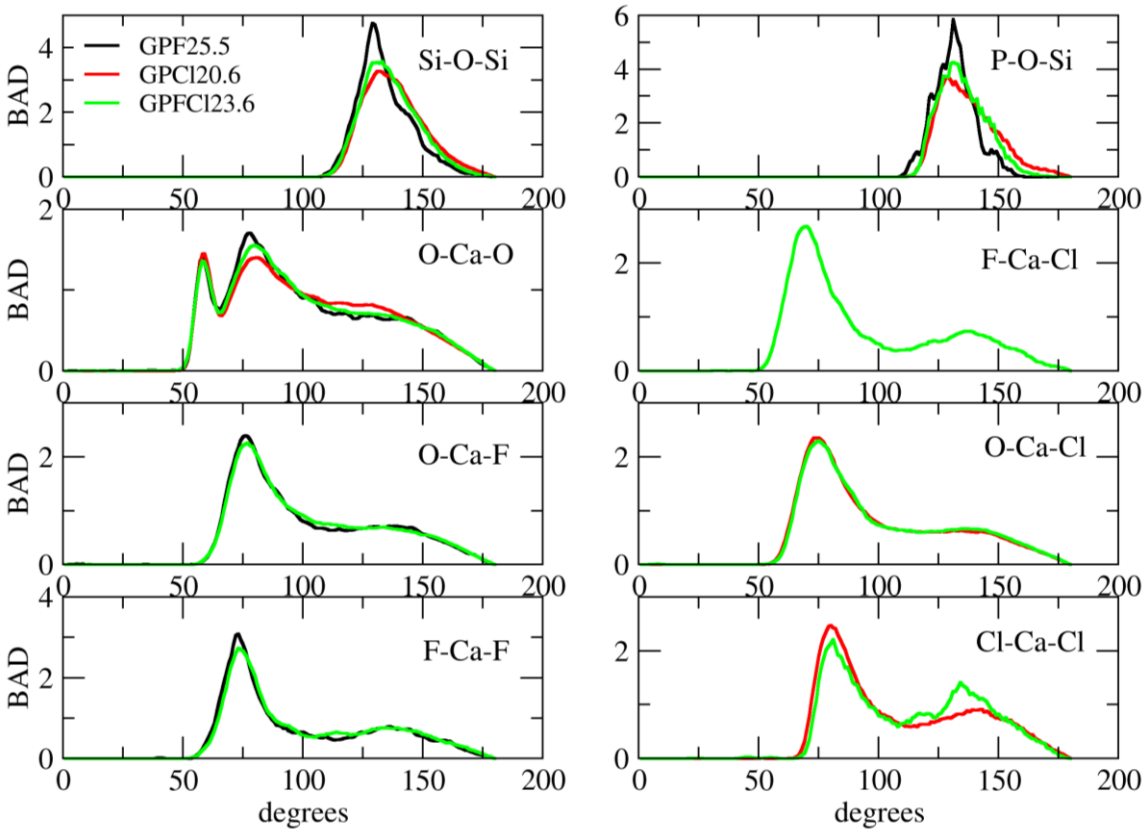

Figure 2. Si-O-Si, P-O-Si and O/F/Cl-Ca-O/F/Cl bond angle distributions (BADs) of the GPF 25.5, GPCl 20.6 and GPFCl23.6 glasses.

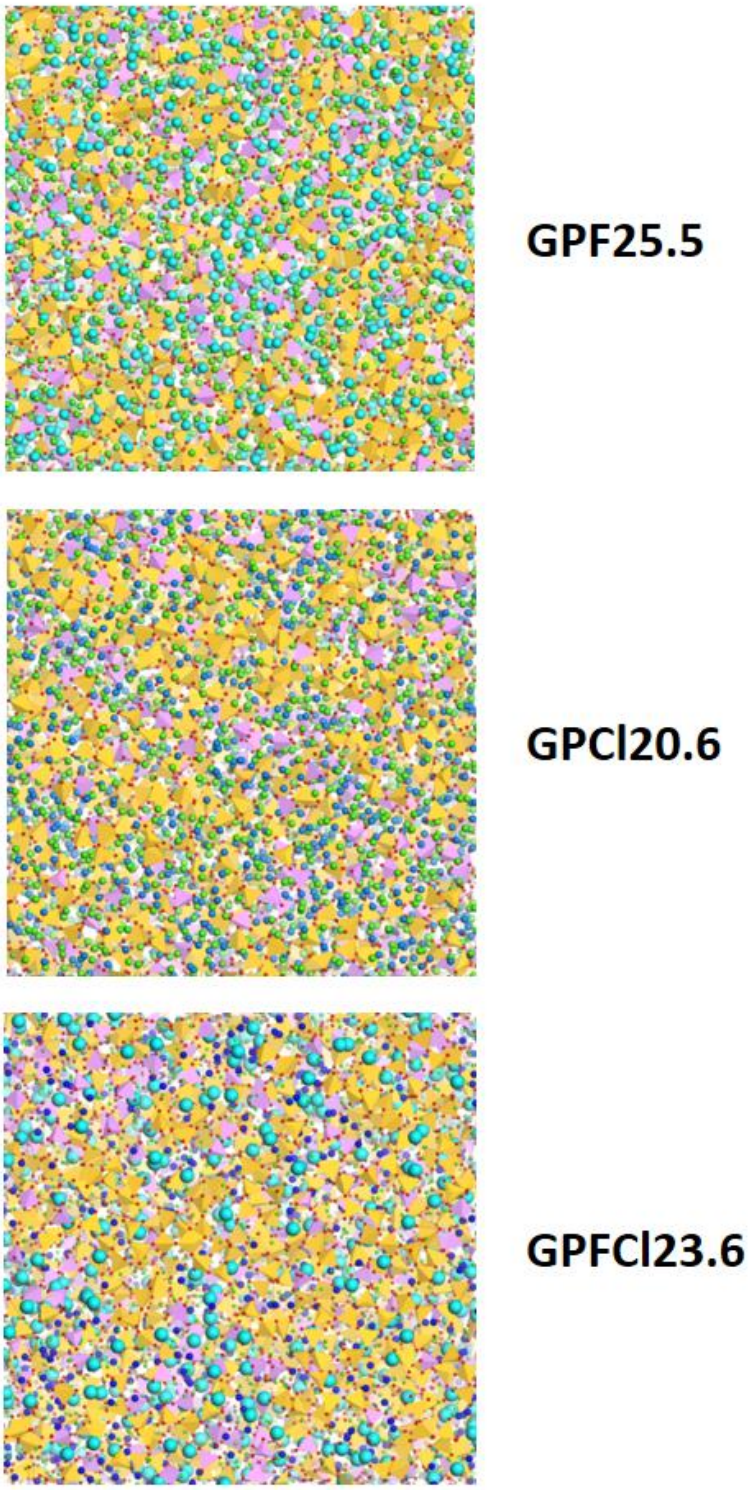

Figure 3. MD derived structural models of GPF25.5, GPCl20.6 and GPFCl23.6 glasses. Yellow and Violet tetrahedral represent SiO_4 and PO_4 units whereas green, blue and cyan spheres represent Ca, F and Cl ions respectively.

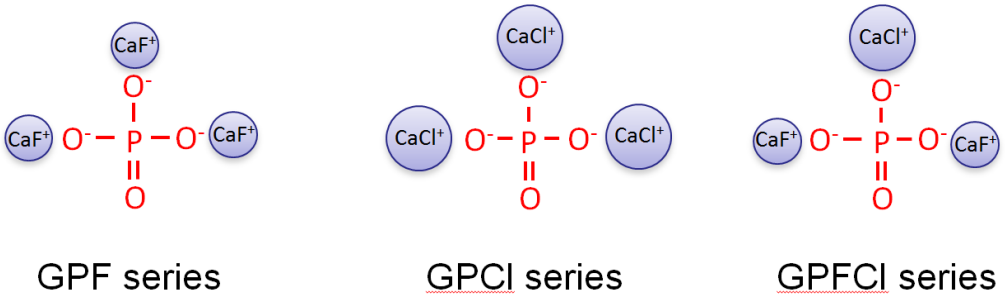

GPF series GPCl series GPFCl series

Figure 4. The potential environment of orthophosphate in oxyhalide containing glass series

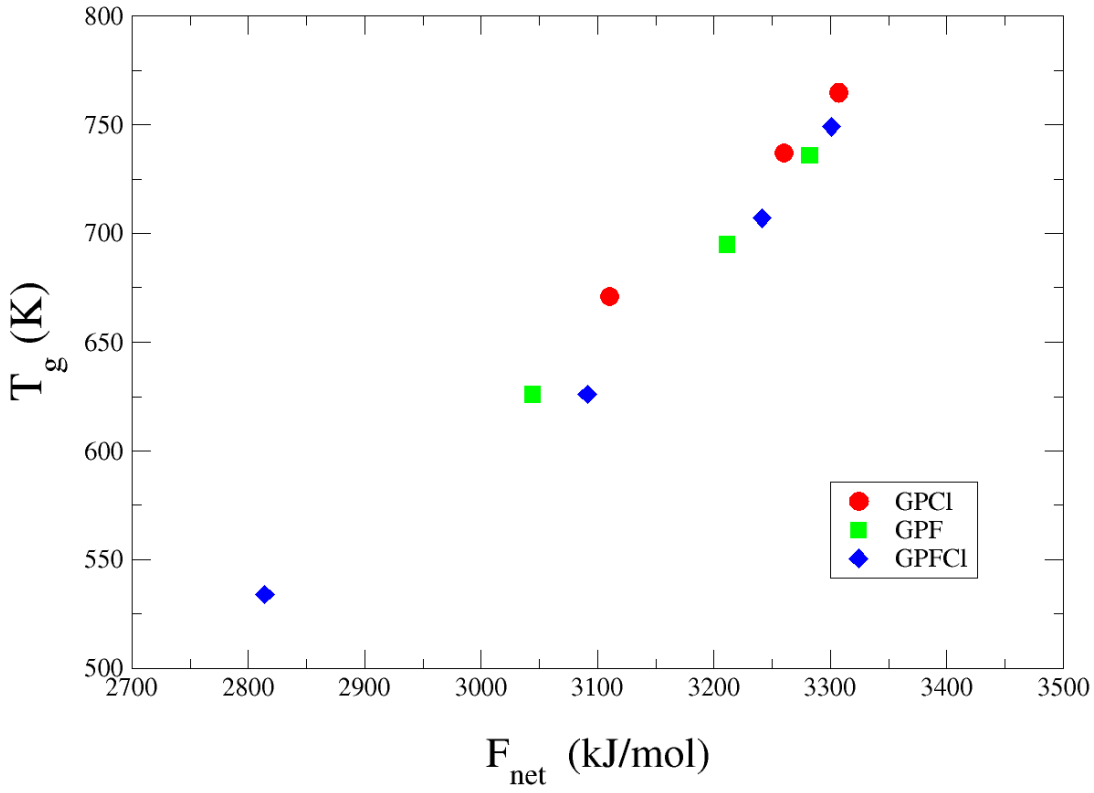

Figure 5. Correlation between the F_{net} factor and the experimental glass transition temperature (T_g) of the investigated glasses.

Table 1. Compositions (mol%) of the glasses simulated, experimental densities, number of atoms in simulation boxes ($N_{atm,MD}$).

Glass	SiO_2	CaO	P_2O_5	CaF_2	$CaCl_2$	Density ($g \cdot cm^3$)	$N_{atm,MD}$
GPF3.0	37.0	53.9	6.1	3.0		2.93	**9999**
GPF6.0	35.9	52.2	5.9	6.0		2.94	**10001**
GPF13.6	32.9	48.0	5.5	13.6		2.98	**9999**
GPF25.5	28.4	41.4	4.7	25.5		3.00	**10002**
GPCl2.3	37.5	54.6	6.2		1.7	2.93	**10010**
GPCl4.6	36.7	53.4	6.0		3.9	2.92	**10010**
GPCl10.6	34.7	50.4	5.8		9.1	2.87	**9990**
GPCl20.6	31.5	45.9	5.2		17.4	2.82	**10000**
GPFCl2.6	37.2	54.2	6.1	1.5	0.9	2.92	**10066**
GPFCl5.3	36.3	52.8	6.0	3.0	1.9	2.93	**10143**
GPFCl12.1	33.8	49.3	5.6	7.0	4.3	2.93	**10323**
GPFCl23.6	29.9	43.6	4.9	13.4	8.1	2.90	**10626**

Table 2. Shell model interatomic potential: analytic functions and parameters. Atomic charges are reported as superscript text.

	Potential forms and parameters		
	Buckingham $Ae^{-r/\rho} - C/r^6$		
	A (eV)	**ρ (Å)**	**C (eV Å^6)**
$O_s^{-2.8482}$–$O_s^{-2.8482}$	22764.30	0.1490	27.88
$F_s^{-1.405}$– $F_s^{-1.405}$	1127.7	0.2753	0.0
$O_s^{-2.8482}$– $F_s^{-1.405}$	8286.91	0.2585	62.2
Si^{4+}–$O_s^{-2.8482}$	8286.91	0.2585	62.20
P^{5+}–$O_s^{-2.8482}$	1142.6775	0.29912	0.0
Si^{4+}–$F_s^{-1.405}$	1143.41168	0.281688	0.0
P^{5+}–$F_s^{-1.405}$	2517.70174	0.235725	0.0
Ca^{2+}–$O_s^{-2.8482}$	2152.3566	0.3092270	0.09944
Ca^{2+}–$F_s^{-1.405}$	1914.4064	0.279210	0.099414
$Cl_s^{-1.984}$–$Cl_s^{-1.984}$	60699.9472	0.262857	107.70
$F_s^{-1.405}$– $Cl_s^{-1.984}$	23480.56439	0.261646	117.36881
$O_s^{-2.8482}$–$Cl_s^{-1.984}$	8286.91	0.2585	62.20
Si^{4+}–$Cl_s^{-1.984}$	1954.92695	0.288358	0.096989
P^{5+}–$Cl_s^{-1.984}$	87535.7324	0.178670	0.0
Ca^{2+}–$Cl_s^{-1.9848}$	3205.18765	0.309210	0.099414
	Three-body potential $\frac{1}{2}k_b(\theta-\theta_0)^2 \exp(-[r_{12}/\rho + r_{13}/\rho])$		
	k_b (eV rad^{-2})	**θ_0 (deg)**	**ρ (Å)**
$O_s^{-2.8482}$–Si^{4+}–$O_s^{-2.8482}$	100.0	109.47	1.0
$O_s^{-2.8482}$–P^{5+}–$O_s^{-2.8482}$	50.0	109.47	1.0
$Cl_s^{-1.984}$–Si^{4+}– $Cl_s^{-1.984}$	100.0	109.47	1.0
$F_s^{-1.405}$–Si^{4+}– $F_s^{-1.405}$	100.0	109.47	1.0
	Core-shell spring potential $1/2\,k_s r^2$		
	k_s (eV Å^{-2})	**Y(e)**	
$O_c^{+0.8482}$–$O_s^{-2.8482}$	74.92	-2.8482	
$Cl_c^{+0.984}$–$Cl_s^{-1.984}$	56.8	-1.984	
$F_s^{-1.405}$–$F_s^{-1.405}$	93.11	-1.405	

Table 3. Average bond distances and coordination numbers of ions in the investigated glasses.

Glass	Average Bond Distances					Coordination numbers						
	Si-O	**P-O**	**Ca-O**	**Ca-F**	**Ca-Cl**	**Si-O**	**P-O**	**Ca-O**	**Ca-F**	**Ca-Cl**	**F-Ca**	**Cl-Ca**
GPCl2.3	1.62	1.55	2.33		2.77	4.0	4.0	6.1		0.3		4.4
GPCl4.6	1.62	1.55	2.34		2.77	4.0	4.0	5.9		0.6		4.3
GPCl10.6	1.62	1.55	2.33		2.75	4.0	4.0	5.3		1.3		4.3
GPCl20.6	1.62	1.55	2.32		2.74	4.0	4.0	4.4		2.4		4.2
GPF3.0	1.61	1.55	2.33	2.21		4.0	4.0	6.0	0.4		3.4	
GPF6.0	1.61	1.55	2.33	2.22		4.0	4.0	5.7	0.7		3.5	
GPF13.6	1.61	1.55	2.34	2.22		4.0	4.0	5.0	1.5		3.5	
GPF25.5	1.61	1.55	2.34	2.23		4.0	4.0	4.0	2.7		3.6	
GPFCl2.6	1.61	1.55	2.34	2.22	2.74	4.0	4.0	6.1	0.2	0.1	3.4	4.5
GPFCl5.3	1.62	1.55	2.34	2.21	2.74	4.0	4.0	5.8	0.4	0.3	3.4	4.4
GPFCl12.1	1.62	1.55	2.34	2.21	2.75	4.0	4.0	5.2	0.8	0.6	3.4	4.5
GPFCl23.6	1.62	1.55	2.34	2.20	2.77	4.0	4.0	4.1	1.4	1.1	3.5	4.6

(*) Negligible percentages of 3-coordinated Si (<0.08%) and 5-coordinated Si (<0.16%) have been found. A cutoff of 3.0 Å was taken for computing the coordination numbers of Ca-O and Ca-F and F-Ca pairs whereas a cutoff of 3.5 was taken for the Ca-Cl and Cl-Ca pairs.

Table 4. Analysis of (Q^n) populations of Si and P (% of the total amount of Si or P), and network connectivity (NC).

Glass	Q^0	Q^1	Q^2	Q^3	Q^4	NC
			Si			
GPF3.0	1.6	22.2	51.5	22.3	2.4	2.02
GPF6.0	1.7	22.2	51.9	22.3	1.9	2.01
GPF13.6	1.4	23.0	50.2	23.3	2.1	2.02
GPF25.5	2.0	21.1	52.2	22.9	1.9	2.02
GPCl2.3	0.9	21.3	52.8	23.5	1.6	2.03
GPCl4.6	1.7	22.7	51.4	22.0	2.2	2.00
GPCl10.6	1.4	22.8	51.5	22.8	1.6	2.00
GPCl20.6	1.9	22.7	51.3	22.2	1.8	2.00
GPFCl2.6	0.8	24.2	50.6	22.4	2.0	2.01
GPFCl5.3	1.1	22.7	51.7	22.6	1.8	2.01
GPFCl12.1	1.6	22.6	52.5	21.1	2.1	1.99
GPFCl23.6	1.4	23.4	50.6	22.9	1.7	2.00
			P			
GPF3.0	82.0	17.5	0.4	0.0	-	0.18
GPF6.0	77.8	22.2	0.0	0.0	-	0.22
GPF13.6	79.1	23.0	0.5	0.0	-	0.24
GPF25.5	81.7	18.0	0.3	0.0	-	0.19
GPCl2.3	80.5	18.5	1.0	0.0	-	0.21
GPCl4.6	78.9	20.5	0.7	0.0	-	0.22
GPCl10.6	75.0	23.3	1.6	0.0	-	0.27
GPCl20.6	72.5	26.4	1.0	0.0	-	0.29
GPFCl2.6	80.0	19.1	0.9	0.0	-	0.21
GPFCl5.3	78.4	21.4	0.2	0.0	-	0.22
GPFCl12.1	77.3	22.0	0.7	0.0	-	0.23
GPFCl23.6	79.9	19.3	0.8	0.0	-	0.21

Table 5. Average CN of the second coordination sphere of ions in the investigated glasses.

Glasses	Si-Ca	P-Ca	Si-F	P-F	Si-Cl	P-Cl	Ca-Si	Ca-P	F-Si	F-P	Cl-Si	Cl-P
GPF3.0	7.9	8.9	0.9	1.0	-	-	5.1	1.9	5.5	2.1	-	-
GPF6.0	8.0	9.0	1.7	2.1	-	-	4.9	1.8	5.1	2.1	-	-
GPF13.6	8.2	9.4	3.7	4.8	-	-	4.4	1.7	4.4	2.0	-	-
GPF25.5	8.2	9.8	6.5	8.5	-	-	3.6	1.4	3.6	1.6	-	-
GPCl2.3	7.7	8.7	-	-	0.5	0.7	5.2	1.9	-	-	4.9	2.5
GPCl4.6	7.8	8.5	-	-	1.1	1.3	5.0	1.8	-	-	5.2	1.9
GPCl10.6	7.7	8.5	-	-	2.5	3.4	4.4	1.7	-	-	4.4	2.2
GPCl20.6	7.5	8.3	-	-	4.4	5.6	3.7	1.4	-	-	3.9	1.7
GPFCl2.6	7.8	8.7	0.4	0.6	0.3	0.3	5.1	1.9	5.1	2.3	5.2	2.0
GPFCl5.3	7.9	8.8	0.8	1.1	0.6	0.5	5.0	1.8	2.2	4.8	0.3	0.9
GPFCl12.1	7.9	9.0	1.9	2.4	1.4	1.1	4.0	1.7	4.5	1.9	1.8	4.5
GPFCl23.6	8.0	9.1	3.2	4.4	2.6	2.0	3.7	1.4	3.5	1.6	1.6	3.7

TOC Graphic